applied sciences

MDPI

Article

Study on Elastic Global Shear Buckling of Curved Girders with Corrugated Steel Webs: Theoretical Analysis and FE Modelling

Kangjian Wang [1], Man Zhou [1,2,*], Mostafa Fahmi Hassanein [3], Jitao Zhong [4], Hanshan Ding [1] and Lin An [5]

1 School of Civil Engineering, Southeast University, Nanjing 210096, China; wangkjw@163.com (K.W.); 230139098@seu.edu.cn (H.D.)
2 School of Civil Engineering, Central South University, Changsha 410075, China
3 Department of Structural Engineering, Faculty of Engineering, Tanta University, Tanta 999060, Egypt; mostafa.fahmi@yahoo.com
4 College of Civil Engineering and Architecture, Shandong University of Science and Technology, Qingdao 271019, China; zhongjitao@126.com
5 Department of Civil Earth Resources Engineering, Kyoto University, Kyoto 615-8540, Japan; an.lin.4w@kyoto-u.ac.jp
* Correspondence: civilzm1988@163.com; Tel.: +86-152-5186-7705

Received: 1 November 2018; Accepted: 28 November 2018; Published: 2 December 2018

Abstract: Despite the construction of several curved prestressed concrete girder bridges with corrugated steel webs (CSWs) around the world; their shear behavior has seldom been investigated. Accordingly, this paper substitutes the lack of available information on the global elastic shear buckling of a plane curved corrugated steel web (PCCSW) in a curved girder. This is based on the equilibrium equations and geometric equations in the elastic theory of classical shells, combined with the constitutive relation of orthotropic shells. Currently, the global elastic shear buckling process of the PCCSW in a curved girder is studied, for the first time in literature, with an equivalent orthotropic open circular cylindrical shell (OOCCS) model. The governing differential equation of global elastic shear buckling of the PCCSW, as well as its buckling strength, is derived by considering the orthotropic characteristics of a corrugated steel web, the rational trigonometric displacement modes, Galerkin's method and variational principles. Additionally, the accuracy of the proposed theoretical formula is verified by comparison with finite element (FE) results. Moreover, the expressions of the inner or outer folded angle and radius of curvature are given by the cosine theorem of the trigonometric function and inverse trigonometric function. Subsequently, parametric analysis of the shear buckling behavior of the PCCSW is carried out by considering the cases where the radius of curvature is constant or variable. This parametric analysis highlights the effects of web dimensions, height-to-thickness ratio, aspect ratios of longitudinal and inclined panels, corrugation height, curvature radius and folded angles on the elastic shear buckling strength. As a result, this study provides a theoretical reference for the design and application of composite curved girders with CSWs.

Keywords: curved girder; curvature radius; corrugated steel web; global shear buckling; Galerkin's method; variational principle

1. Introduction

The prestressed concrete girder bridge with corrugated steel webs (CSWs) is a novel type of composite structure. It is made with a folded steel web and concrete flanges. Accordingly, it combines

the advantages of the mechanical properties of both concrete and steel and significantly increases the structural strength-to-weight ratio. Compared with traditional concrete webs, CSWs can solve the problem of web cracking and improve, to some extent, the span capacity. This novel structure, indeed, has many other advantages, such as low manufacturing cost, high prestressing efficiency and convenience for assembly construction. As a novel composite thin-walled structure, bridge girders with CSWs date back to the 1980s when the first bridge was constructed in France. They were widely applied in Japan soon afterward [1], such as the Shirasawa Bridge and Shintogawa Bridge shown in Figure 1 with a certain horizontal curvature. Since 2005, prestressed concrete girders with CSWs have been vigorously promoted in China, e.g., the Yuwotou curved girder bridge of Guangzhou Province and No. 3 East River curved bridge located in Sichuan Province. With the maturing of design theory of bridge girders with CSWs and improvement of the level of manufacture and construction, this new type of bridge is becoming increasingly competitive in medium and large bridge construction. Thus, CSWs can widely be used for highways, viaducts, and ramp girder bridges, adding a beautiful curvilinear appearance.

(**a**) (**b**)

Figure 1. Shintogawa Bridge in Japan (completed in 2013): (**a**) Top view; (**b**) Side view. CSWs: corrugated steel webs. CSWs: corrugated steel webs.

As a type of a thin-walled structure, shear buckling is the controlling factor in the design process of beams with CSWs. Thus, many scholars have studied their buckling behavior, including local and global buckling, of prismatic girders with CSWs [2–12]. The global elastic shear buckling stress formulas of corrugated webs were given by Easley [13] and Galambos [14] considering different buckling factors, and later, the formulas were applied to prismatic or non-prismatic girders with CSWs [15]. Based on a series of experiments, Hamilton (1993) [2], and Sayed-Ahmed (2005) [3] held the view that shear forces were mainly carried by CSWs and that structural failure was caused by shear buckling of the steel web. Johnson (1997) found that stress in the CSW is generated only by the vertical shear forces, while the shrinkage, creep, prestressing and temperature of the upper and lower concrete flanges have little effect on the web [4]. Hassanein et al. (2014, 2015, 2016) performed a theoretical study, primarily on the shear buckling behavior of tapered bridge girders with CSWs, and then obtained a strength design formula for these webs [15–17]. Subsequently, Hassanein et al. (2017) numerically presented the nonlinear shear buckling response combined with the advantages of both high-strength steel and bridge girder with CSWs [18]. Leblouba et al. (2017) experimentally and numerically studied the shear behavior of trapezoidal corrugated webs from the pre-buckling stage until ultimate failure [19]. Based on experimental and theoretical analysis, Zhou et al. (2016) first studied the shear stress distribution and shear deformation in non-prismatic beams with CSWs [20–22]. On the other hand, Basher et al. [23] studied the nonlinear shear strength of curved composite plate girders with CSWs. The girders were assumed straight, in the first step of their design model, and the shear strengths of the girders were taken as the sum of the web buckling load, the web post buckling strength and the flanges contribution, besides that of the concrete slab. Then, this strength was extended to the curved girders with CSWs by applying a modification factor that considers the

bending of the curved girders. From the authors' view point, obtaining the buckling load of the curved CSW would better be presented based on theoretical derivations than just applying a modification factor to the straight web configuration. Note that some new research fields were extended in recent years, for instance, Bedon investigated the buckling behavior of timber log-walls and other composite structures through theoretical analysis and finite element simulation [24,25].

From the aforementioned research, it could be drawn that these studies involving only the shear buckling of straight girders with CSWs have made some progress and are constantly improving, but few studies have focused on the shear behavior of curved girders with CSWs. However, the mechanical behavior of curved girders with CSWs is quite different from that of straight girders due to the effect of the initial curvature or curvature radius and corrugation dimensions or folded angles. In addition, the bearing capacity of the structure is controlled by shear failure, and the bridge is in an elastic stage during construction and operation. Therefore, it is of great significance to determine the global elastic shear buckling strength of the plane curved corrugated steel web (PCCSW) with respect to both theory and engineering practice, instead of just applying a modification factor for the buckling values of straight webs. Moreover, in this study, the authors conducted preliminary theoretical and numerical studies on the global elastic shear buckling of PCCSWs in bridge girders. The results indicated that the global elastic shear buckling is more prominent in curved girders. Accordingly, this paper gives the complete data under overall elastic shear buckling conditions of CSWs in curved girders.

2. Basic Equations

The mechanical properties of engineering structures including novel bridge girders with CSWs are closely related to mechanics, especially the elastic response of bridges. For thin-walled shells used in engineering, the force distribution diagram of an orthotropic open cylindrical shell element is illustrated in Figure 2; the diagram shows a thin-walled structure considering the membrane effect. From the classical elasticity theory, the equilibrium equation, geometric equation and constitutive relation of an orthotropic open circular cylindrical shell (OOCCS) can be obtained:

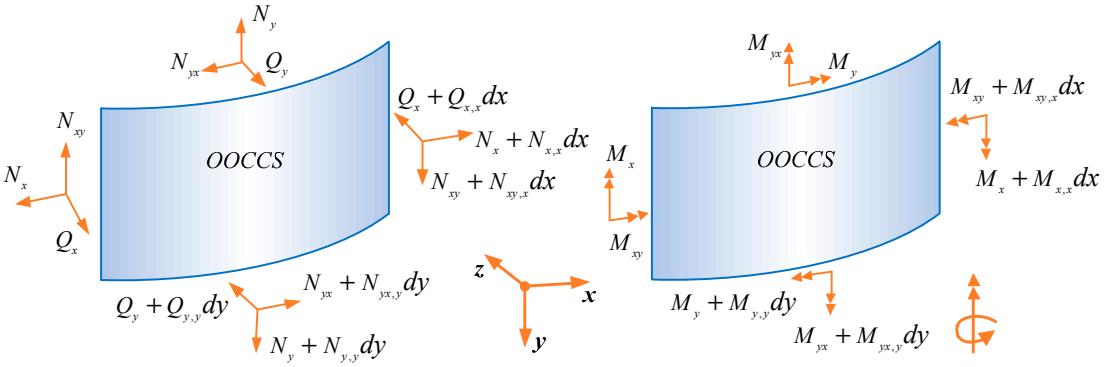

(a) Force of translation (b) Moment of rotation

Figure 2. Force distribution diagram of an orthotropic open cylindrical shell element. OOCCS: orthotropic open circular cylindrical shell.

Equilibrium differential equations:

$$\frac{\partial N_x}{\partial x} + \frac{\partial N_{yx}}{\partial y} = 0 \tag{1}$$

$$\frac{\partial N_{xy}}{\partial x} + \frac{\partial N_y}{\partial y} = 0 \tag{2}$$

$$\frac{\partial Q_x}{\partial x} + \frac{\partial Q_y}{\partial y} + N_x\left(\frac{1}{R} + \frac{\partial^2 w}{\partial x^2}\right) + N_y\frac{\partial^2 w}{\partial y^2} + N_{xy}\frac{\partial^2 w}{\partial x \partial y} + N_{yx}\frac{\partial^2 w}{\partial x \partial y} = 0 \tag{3}$$

$$\frac{\partial M_x}{\partial x} + \frac{\partial M_{yx}}{\partial y} - Q_x = 0 \tag{4}$$

$$\frac{\partial M_{xy}}{\partial x} + \frac{\partial M_y}{\partial y} - Q_y = 0 \tag{5}$$

Deformation geometric equations:

$$\varepsilon_x = \frac{\partial u}{\partial x} - \frac{1}{R}w + \frac{1}{2}\left(\frac{\partial w}{\partial x}\right)^2, \varepsilon_y = \frac{\partial v}{\partial y} + \frac{1}{2}\left(\frac{\partial w}{\partial y}\right)^2, \gamma_{xy} = \frac{\partial u}{\partial y} + \frac{\partial v}{\partial x} + \frac{\partial w}{\partial x}\frac{\partial w}{\partial y} \tag{6}$$

Orthotropic constitutive equations:

$$\varepsilon_x = \frac{\sigma_x}{E_x} - \nu_y\frac{\sigma_y}{E_y}, \varepsilon_y = \frac{\sigma_y}{E_y} - \nu_x\frac{\sigma_x}{E_x}, \gamma_{xy} = \frac{2(1+\nu)}{E}\tau_{xy} \tag{7}$$

where xyz denotes the cylindrical coordinate system, and the x-, y- and z-axes are the circumferential, vertical and radial directions, respectively. σ_x, σ_y and τ_{xy} are the normal and shear stresses, respectively. ε_x and ε_y are the normal strains in the x-direction and y-direction, respectively, and γ_{xy} is the shear strains. u, v and w are the circumferential, vertical and radial displacements, respectively. R is the radius of curvature. E_x and E_y are the Young's moduli in the x-direction and y-direction, respectively, and ν_x and ν_y are the Poisson's ratios in the x- and y-direction, respectively. Q_x and Q_y are the radial shear forces per unit length in the x-direction and y-direction, respectively. M_x and M_y are the bending moments per unit length in the x- and y-direction, respectively. N_x and N_y are the normal forces per unit length in the x-direction and y-direction and are defined as $N_x = t\sigma_x$ and $N_y = t\sigma_y$, respectively. M_{xy} and M_{yx} are the twisting moments per unit length that satisfy the reciprocal theorem of torsion moment, that is, $M_{xy} = M_{yx}$. N_{xy} and N_{yx} are the membrane shear forces in the x-y plane per unit length that meet the shear stress reciprocal principle, namely, $N_{xy} = N_{yx} = t\tau_{xy} = t\tau_{yx}$, where t is the plate thickness. $w = w(x, y)$ is a function depending on x and y. The relationships between the elastic constants of orthotropic materials are $\nu_x/\nu_y = E_x/E_y$, $E = \sqrt{E_x E_y}$ and $\nu = \sqrt{\nu_x \nu_y}$. In addition, $u = -z\frac{\partial w}{\partial x}$ and $v = -z\frac{\partial w}{\partial y}$.

3. Derivation of the Governing Equations

Based on the above basic equations of classical elastic shell theory and orthotropic shell theory, the corresponding deformation compatibility equation of equivalent anisotropic shells is derived from the geometric equations given above in Equation (6):

$$\frac{\partial^2 \varepsilon_x}{\partial y^2} + \frac{\partial^2 \varepsilon_y}{\partial x^2} - \frac{\partial^2 \gamma_{xy}}{\partial x \partial y} = \left(\frac{\partial^2 w}{\partial x \partial y}\right)^2 - \frac{\partial^2 w}{\partial x^2}\frac{\partial^2 w}{\partial y^2} - \frac{1}{R}\frac{\partial^2 w}{\partial y^2} \tag{8}$$

The internal force of the shell can be obtained by the integration of the stress in the cross section expressed as the relation with displacement. Equation (9) is the displacement expression of the bending (M_x and M_y) or torsional moment:

$$M_x = -D_x\left(\frac{\partial^2 w}{\partial x^2} + \nu_y\frac{\partial^2 w}{\partial y^2}\right), M_y = -D_y\left(\frac{\partial^2 w}{\partial y^2} + \nu_x\frac{\partial^2 w}{\partial x^2}\right), M_{xy} = -\frac{Et^3}{12(1+\nu)}\frac{\partial^2 w}{\partial x \partial y} \tag{9}$$

where D_x and D_y are the equivalent flexural stiffness in the x- and y-direction per unit length, respectively. $D_x = \frac{E_x t^3}{12(1-\nu_x\nu_y)}$, and $D_y = \frac{E_y t^3}{12(1-\nu_x\nu_y)}$. This equation indicates that the equivalent shell is different from the isotropic shell in the physical mechanism, and the differences in the elastic modulus and Poisson's ratio are reflected in the two perpendicular directions (i.e., the tangential and vertical directions) from the physical angle, which can further reflect the flexural rigidity in two directions.

Substituting Equation (9) into Equations (4) and (5), the following equations concerning displacement expressions of shear forces can be obtained:

$$Q_x = -\frac{\partial}{\partial x}(D_x\frac{\partial^2 w}{\partial x^2} + \frac{D_{xy}}{2}\frac{\partial^2 w}{\partial y^2}), Q_y = -\frac{\partial}{\partial y}(\frac{D_{xy}}{2}\frac{\partial^2 w}{\partial x^2} + D_y\frac{\partial^2 w}{\partial y^2}) \tag{10}$$

where D_{xy} is the equivalent torsional stiffness in the x-y plane per unit length; $D_{xy} = 2\nu_y D_x + \frac{Et^3}{6(1+\nu)}$.

Let ϕ be an Airy stress function, satisfying Equations (1) and (2); then, we can obtain

$$\sigma_x = \frac{\partial^2 \phi}{\partial y^2}, \sigma_y = \frac{\partial^2 \phi}{\partial x^2}, \tau_{xy} = -\frac{\partial^2 \phi}{\partial x \partial y} \tag{11}$$

Substituting the shear force expression of Equation (10) into Equation (3), the following equation can be obtained:

$$D_x\frac{\partial^4 w}{\partial x^4} + D_{xy}\frac{\partial^4 w}{\partial x^2 \partial y^2} + D_y\frac{\partial^4 w}{\partial y^4} = t\sigma_x(\frac{1}{R} + \frac{\partial^2 w}{\partial x^2}) + t\sigma_y\frac{\partial^2 w}{\partial y^2} + 2t\tau_{xy}\frac{\partial^2 w}{\partial x \partial y} \tag{12}$$

Applying the strain expression in Equation (7) to Equation (8), the following equation can be obtained:

$$\frac{1}{E_x}\frac{\partial^2 \sigma_x}{\partial y^2} + \frac{1}{E_y}\frac{\partial^2 \sigma_y}{\partial x^2} - \frac{2}{E}\frac{\partial^2 \tau_{xy}}{\partial x \partial y} - \frac{\nu}{E}(\frac{\partial^2 \sigma_y}{\partial y^2} + 2\frac{\partial^2 \tau_{xy}}{\partial x \partial y} + \frac{\partial^2 \sigma_x}{\partial x^2}) = (\frac{\partial^2 w}{\partial x \partial y})^2 - \frac{\partial^2 w}{\partial x^2}\frac{\partial^2 w}{\partial y^2} - \frac{1}{R}\frac{\partial^2 w}{\partial y^2} \tag{13}$$

Using Equation (11), Equations (12) and (13) become

$$D_x\frac{\partial^4 w}{\partial x^4} + D_{xy}\frac{\partial^4 w}{\partial x^2 \partial y^2} + D_y\frac{\partial^4 w}{\partial y^4} = tL(w, \sigma) + \frac{t}{R}\frac{\partial^2 \phi}{\partial y^2} \tag{14}$$

$$\frac{1}{E_x}\frac{\partial^4 \phi}{\partial y^4} + \frac{1}{E_y}\frac{\partial^4 \phi}{\partial x^4} + \frac{2}{E}\frac{\partial^4 \phi}{\partial x^2 \partial y^2} = S(w, w) - \frac{1}{R}\frac{\partial^2 w}{\partial y^2} \tag{15}$$

where $L(w, \sigma)$ is a nonlinear term, and $S(w, w)$ is a higher order term.

$$L(w, \sigma) = \sigma_x\frac{\partial^2 w}{\partial x^2} + \sigma_y\frac{\partial^2 w}{\partial y^2} + 2\tau_{xy}\frac{\partial^2 w}{\partial x \partial y}, \; S(w, w) = (\frac{\partial^2 w}{\partial x \partial y})^2 - \frac{\partial^2 w}{\partial x^2}\frac{\partial^2 w}{\partial y^2} \tag{16}$$

Due to the external forces per unit thickness of the shell boundary causing the principal compressive stresses p_x, p_y and p_{xy}, the following equations can be obtained:

$$p_x = -\sigma_x, p_y = -\sigma_y, p_{xy} = -\tau_{xy} \tag{17}$$

4. Formulation of the Problem

Currently, the plane curved CSW of composite curved girder bridges is considered as an orthotropic open circular cylindrical shell, and equivalent orthogonal open cylindrical shell can be regarded as a continuous, homogeneous, orthotropic and perfectly elastic body, as shown in Figure 3. Applying Equation (17) to the nonlinear term in Equation (14) and only considering the pure shear state results in $P_{xy} = tp_{xy} = -t\tau_{xy}$. Then neglecting the higher order term in Equation (15), the global elastic shear buckling control differential equation of a PCCSW can be written as follows:

$$D_x\frac{\partial^4 w}{\partial x^4} + D_{xy}\frac{\partial^4 w}{\partial x^2 \partial y^2} + D_y\frac{\partial^4 w}{\partial y^4} + 2P_{xy}\frac{\partial^2 w}{\partial x \partial y} - \frac{t}{R}\frac{\partial^2 \phi}{\partial y^2} = 0 \tag{18}$$

$$\frac{1}{E_x}\frac{\partial^4 \phi}{\partial y^4} + \frac{1}{E_y}\frac{\partial^4 \phi}{\partial x^4} + \frac{2}{E}\frac{\partial^4 \phi}{\partial x^2 \partial y^2} + \frac{1}{R}\frac{\partial^2 w}{\partial y^2} = 0 \tag{19}$$

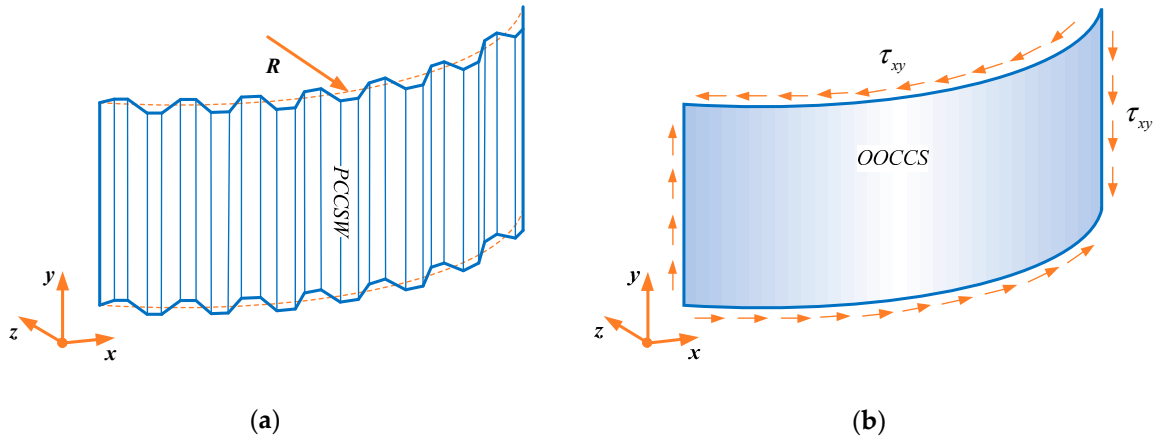

Figure 3. Plane curved CSW and its equivalent model: (**a**) Plane curved corrugated steel web; (**b**) Equivalent orthotropic shell. PCCSW: plane curved corrugated steel web.

The governing differential Equations (18) and (19) can be reduced to an isotropic cylindrical shell equation, that is, a Donnell equation [26], which shows the rationality of the governing differential equations. In addition, the equivalent stiffness of the CSW used in the design guideline for composite bridges in Japan can be expressed as follows [27]:

$$\begin{aligned} D_x &= \frac{E_s t^3}{12(1-\nu_s{}^2)} \\ D_y &= \frac{s}{l}\frac{E_s(t^3+th_r{}^2)}{6} \\ D_{xy} &= \frac{s}{l}\frac{E_s t^3}{6(1+\nu_s)} \end{aligned} \tag{20}$$

Here, E_s and ν_s are the elastic modulus and Poisson's ratio of steel, respectively, h_r is the corrugation depth of the CSW, s is the total folded panel segment length of single periodic corrugation, and l is the projection length of s in relation to the longitudinal curved axis.

5. Solution of the Governing Differential Equations

Equations (18) and (19) can be combined into an eight-order differential equation with different bending stiffnesses and elastic moduli with regard to curvature radius. The mathematical software MAPLE (Maple V, Waterloo Maple Inc., Waterloo, Ontario Prov., Canada and 2012) [28] is used in subsequent calculations, which can accurately be used to perform differential and integration operations.

5.1. Displacement Model and the Galerkin Method

Note that if the arc length of the equivalent elastic shell is greater than the height, the buckling value remains stable. This is because the buckling value is independent of the length, especially the long narrow shells [16,29]. According to the deflection surface function of a long narrow shell, considering the distance between the intersegmental lines on both sides of the global shear buckling semiwave surface λ, the slope of intersegmental line β, and shell height H, the deflection surface equation and the stress function expression of a simply supported boundary shell are as follows:

$$w = Asin\frac{\pi}{\lambda}(x-\beta y)sin\frac{\pi y}{H} \tag{21}$$

$$\phi = Bsin\frac{\pi}{\lambda}(x-\beta y)sin\frac{\pi y}{H} \tag{22}$$

On the basis of the mathematical model formed by differential Equations (18) and (19) and displacement Equations (21) and (22), the Galerkin method is used based on the principle of virtual

displacement, namely, the work done by the generalized force (Equations (18) and (19)) on the generalized virtual displacement (Equations (21) and (22)), respectively, is zero.

$$\int_0^\lambda \int_0^H \left[(D_x \frac{\partial^4 w}{\partial x^4} + D_{xy} \frac{\partial^4 w}{\partial x^2 \partial y^2} + D_y \frac{\partial^4 w}{\partial y^4}) + 2P_{xy} \frac{\partial^2 w}{\partial x \partial y} - \frac{B}{A} \frac{t}{R} \frac{\partial^2 \phi}{\partial y^2} \right] sin \frac{\pi}{\lambda}(x - \beta y) sin \frac{\pi y}{H} \delta A dx dy = 0 \tag{23}$$

$$\int_0^\lambda \int_0^H \left(\frac{1}{E_x} \frac{\partial^4 \phi}{\partial y^4} + \frac{1}{E_y} \frac{\partial^4 \phi}{\partial x^4} + \frac{2}{E} \frac{\partial^4 \phi}{\partial x^2 \partial y^2} + \frac{A}{B} \frac{1}{R} \frac{\partial^2 w}{\partial y^2} \right) sin \frac{\pi}{\lambda}(x - \beta y) sin \frac{\pi y}{H} \delta B dx dy = 0 \tag{24}$$

where δ is a variational operator. Due to variation, δA and δB are arbitrary and they not equal to zero. Thus:

$$\int_0^\lambda \int_0^H sin \frac{\pi}{\lambda}(x - \beta y) sin \frac{\pi y}{H} \left[(D_x \frac{\partial^4 w}{\partial x^4} + D_{xy} \frac{\partial^4 w}{\partial x^2 \partial y^2} + D_y \frac{\partial^4 w}{\partial y^4}) + 2P_{xy} \frac{\partial^2 w}{\partial x \partial y} - \frac{B}{A} \frac{t}{R} \frac{\partial^2 \phi}{\partial y^2} \right] dx dy = 0 \tag{25}$$

$$\int_0^\lambda \int_0^H sin \frac{\pi}{\lambda}(x - \beta y) sin \frac{\pi y}{H} \left(\frac{1}{E_x} \frac{\partial^4 \phi}{\partial y^4} + \frac{1}{E_y} \frac{\partial^4 \phi}{\partial x^4} + \frac{2}{E} \frac{\partial^4 \phi}{\partial x^2 \partial y^2} + \frac{A}{B} \frac{1}{R} \frac{\partial^2 w}{\partial y^2} \right) dx dy = 0 \tag{26}$$

According to the orthogonality principle of a trigonometric function, in terms of Equations (21) and (22) and their derivatives, Equation (26) can be expressed as

$$\frac{\pi^2 B}{E_x}(\beta^4 + 6\frac{\beta^2 \lambda^2}{H^2} + \frac{\lambda^4}{H^4}) + \frac{\pi^2 B}{E_y} + \frac{2\pi^2 B}{E}(\beta^2 + \frac{\lambda^2}{H^2}) - \frac{A}{B}\frac{A}{R}(\beta^2 \lambda^2 + \frac{\lambda^4}{H^2}) = 0 \tag{27}$$

Here, $\alpha = \frac{\lambda^2}{H^2}$, $A_0 = \left(\frac{A}{B}\right)^2$; then,

$$A_0 = \left[\frac{\pi^2}{E_x}(\beta^4 + 6\beta^2 \alpha + \alpha^2) + \frac{\pi^2}{E_y} + \frac{2\pi^2}{E}(\beta^2 + \alpha) \right] \frac{R}{H^2(\beta^2 \alpha + \alpha^2)} \tag{28}$$

In terms of the orthogonality principle of a trigonometric function, substituting Equations (21) and (22) and their derivatives into Equation (25), the following equation can similarly be given:

$$P_{xy} = \frac{\pi^2}{2}[\frac{D_x}{\lambda^2 \beta} + D_{xy}(\frac{\beta}{\lambda^2} + \frac{1}{H^2 \beta}) + D_y(\frac{\beta^3}{\lambda^2} + 6\frac{\beta}{H^2} + \frac{\lambda^2}{H^4 \beta})] + \frac{t}{2RA_0}(\beta + \frac{\lambda^2}{H^2 \beta}) \tag{29}$$

5.2. Functional Extremum Value

Since the length of the PCCSWs used in composite curved bridge girders is greater than the height, the height of the global elastic shear buckling semiwave surface is filled with the entire height range of the PCCSW. A variation of the internodal line slope or of the internode distance along the length of the PCCSW is made to obtain the global elastic shear buckling value of the maximum semiwave of the PCCSW. Because it involves the solution of the extremum value, the first-order partial derivatives of P_{xy} with respect to β and λ can be obtained:

$$\frac{\partial P_{xy}}{\partial \beta} = 0 \tag{30}$$

$$\frac{\partial P_{xy}}{\partial \lambda} = 0 \tag{31}$$

By Equation (31), the following equations can be obtained:

$$\alpha = \sqrt{\frac{D_x + D_{xy}\beta^2 + D_y \beta^4}{D_y + \gamma}} \tag{32}$$

$$\gamma = \frac{tH^2}{RA_0 \pi^2} \tag{33}$$

Here, γ can be viewed as the curvature parameter; by Equation (30), the following equation can be obtained:

$$\alpha[\pi^2 RA^2(D_{xy} - 6\beta^2 D_y) - tB^2H^2\beta^2] = \pi^2 RA^2(-D + D_{xy}\beta^2 + 3D_y\beta^4 - D_y\alpha^2) - tB^2H^2\alpha^2 \quad (34)$$

By Equations (32)–(34), the following equation can be obtained:

$$\beta = \left(\frac{\frac{2D_x}{D_y+\gamma} + \frac{D_x D_y}{(D_y+\gamma)^2} + \frac{D_x}{D_y}}{\frac{40D_y}{D_y+\gamma} + 6 - \frac{2{D_y}^2}{(D_y+\gamma)^2}} \right)^{\frac{1}{4}} \quad (35)$$

Substitution of Equations (32) and (35) into Equation (28) and then into Equation (33) allows the following equation to be obtained:

$$\gamma = \frac{5D_x H^4}{2\pi^4 R^2 t^2} \quad (36)$$

Similarly, by applying Equations (32) and (35) to Equation (28) and then to Equation (29), the following equation of the global elastic shear buckling force unit length of the PCCSW can be obtained:

$$P_{xy} = (35.03 + 43.83\frac{\gamma}{D_y} + 8.16\frac{\gamma^2}{{D_y}^2})\frac{{D_x}^{\frac{1}{4}}{D_y}^{\frac{3}{4}}}{H^2} \quad (37)$$

Taking R from Equation (36) to infinity, Equation (37) is transformed into the global elastic shear buckling formula for the CSW used in composite straight girders, which agrees well with the Easley formula [13]. Simultaneously, the accuracy of the algorithm is verified.

6. Numerical Study and Comparison

In this paper, finite element (FE) models of PCCSW are developed using the general application software ANSYS (ANSYS 12.1, ANSYS Inc., Canonsburg, PA, USA and 2012) [30] for the numerical investigation and parametric analysis. In this study, the elastic buckling modes are extracted from the static general models. The results of the theoretical and numerical analysis are then compared.

6.1. Element Type and Material Properties

The quadrilateral finite-membrane-strain shell element (Shell63) with both bending and membrane capabilities was used for modeling the three dimensional model PCCSW without flanges and stiffeners. This general purpose three dimensional reduced integration element with a 4-node elastic thin shell element is an appropriate element for most applications, and it is specified by its thickness. Each node of the element has six degrees of freedom, namely, translational displacements along the x, y and z directions and rotational displacement around each axis. For complex buckling behavior, it provides accurate and reliable solutions. Material properties adopt the elastic stress-strain relationship of steel, as shown in Table 1, and at the same time, the material characteristics of the equivalent orthotropic shell are given.

Table 1. Material constants needed in numerical simulation of Shinkai Bridge [31] as an example. PCCSW: plane curved corrugated steel web; OOCCS: orthotropic open circular cylindrical shell.

PCCSW	OOCCS
$E_s = 2.1 \times 10^5$ MPa $\nu_s = 0.3$	$E_y = 2.33 \times 10^5$ MPa, $E_x = 420$ MPa $\nu_y = 0.3$, $\nu_x = 5.4 \times 10^{-4}$

6.2. Geometry and Mesh

The typical finite element mesh of a PCCSW is shown in Figure 4, which is generated by using lines and areas. Finite element mesh sizes of 80 mm × 80 mm are used for each longitudinal panel and inclined panel of the PCCSW. In the mesh partition stage, the number of elements belong to each panel segment of the PCCSW is more reasonable in the finite element simulation. Additionally, mapped meshing is adopted. Four elements were used for meshing longitudinal and inclined panels due to the transfer of longitudinal loads along the edge of the web from the inclined panel to the longitudinal panel.

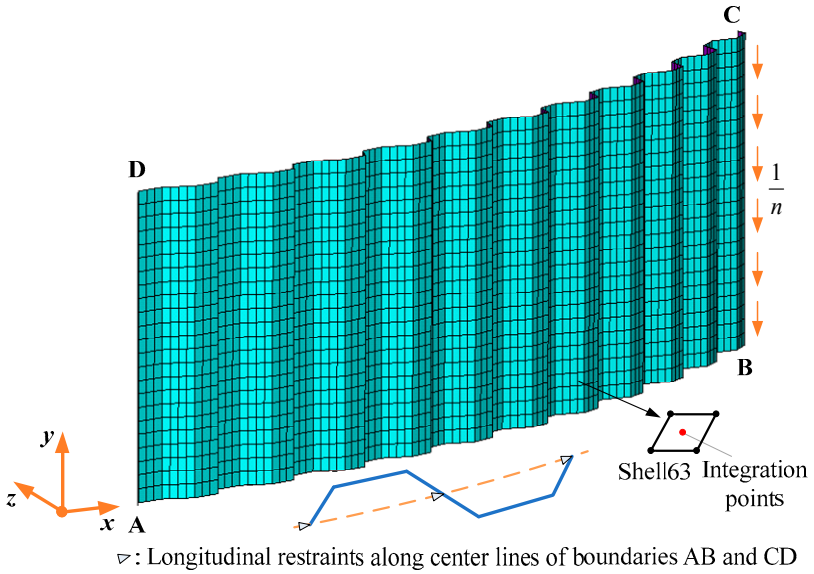

Figure 4. Finite element model of plane curved corrugated steel web (PCCSW).

Numerical analysis using large general-purpose software ANSYS and theoretical verification are performed in the following analysis. The data are shown in the following tables. The finite element model is shown in Figure 4.

6.3. Loading and Boundary Conditions

The PCCSW is prevented from translational movements in some directions, while the rotational displacements are excluded in all directions. The translational restraints of the *AD* and *BC* edges are under the restrained state except in the shear load direction. All the longitudinal and inclined panels of the *AB* and *CD* edges are subjected to radial restraints, and the boundaries of *AB* and *CD* are also subjected to longitudinal restraints at the midpoint of all inclined panels. The shear load is uniformly distributed along edge *BC*. The considered simply supported boundary conditions, representing the lower bound conditions in real bridge girders, are shown in Table 2. It is worth pointing out that these boundary conditions have been verified by the co-author [32] by comparing the critical buckling stresses of flat webs with the theoretical predictions [29].

Table 2. Boundary conditions of the PCCSW (Note: R: Restrained, F: Free).

Boundary	Symbols	AB, CD	AB, CD (Midpoint of Inclined Panel)	AD	BC
Translation	δ_x	F	R	R	R
	δ_y	F	F	R	F
	δ_z	R	F	R	R
Rotation	θ_x	F	F	F	F
	θ_y	F	F	F	F
	θ_z	F	F	F	F

A uniform nodal force is applied along the boundary *BC*. The sum of all nodal forces on the edge is the unit force. Thus, each nodal force is $1/n$, where n is the node number. Figure 5 represents the positive first order global elastic shear buckling mode of the PCCSW, which is the most conservative mode in the structural buckling calculation [17]. The elastic buckling eigenvalue calculated by FEM and the critical buckling value of the finite element can be calculated by:

$$\tau_{cr,F} = \frac{eigenvalue}{tH} \tag{38}$$

where buckling eigenvalue extraction uses the block Lanczos method, and the middle surface value of the shell is extracted by finite element results.

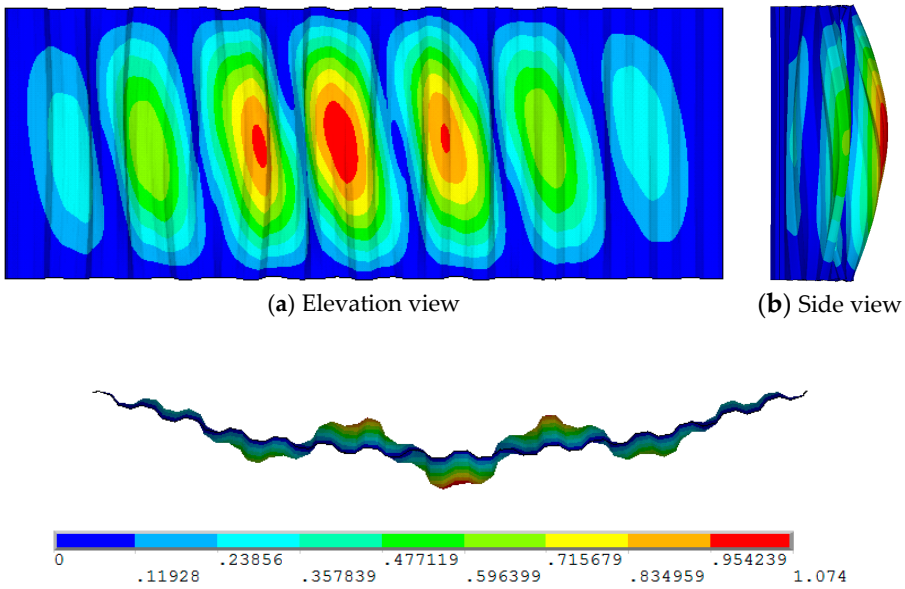

(**a**) Elevation view (**b**) Side view

(**c**) Overhead view

Figure 5. Global elastic shear buckling mode of the PCCSW.

6.4. Trigonometric Relation between the Dimensions of PCCSW

To determine the relationship between the geometric variables of the PCCSW, a single wavelength PCCSW is taken, as shown in Figure 6. Here, s is a single wavelength, l is the projected length of a single wavelength in relation to the longitudinal axis, a is the length of the longitudinal panel, c is the length of the inclined panel, b is the projected length of the inclined panel in relation to the longitudinal axis, R is the radius of curvature, h_r is the amplitude height of the PCCSW, t is the panel thickness, θ is the angle of the inclined panel in relation to the tangent line of the longitudinal axis, θ_1 is the outer folded angle, θ_2 is the inner folded angle, and α_1, α_2, α_3, α_4 and α_5 are all auxiliary angles. Because of the difference between the inside and outside folded angles, the curved shape appearance of the PCCSW is formed.

The following equations (expressions about a, R, h_r and c) are obtained in accordance with the triangle cosine theorem:

$$cos\alpha_1 = \frac{a}{2(R + h_r/2)} \tag{39}$$

$$cos\alpha_2 = \frac{c^2 + 2Rh_r}{2c(R + h_r/2)} \tag{40}$$

$$cos\alpha_3 = \frac{c^2 - 2Rh_r}{2c(R - h_r/2)} \tag{41}$$

$$cos\alpha_4 = \frac{a}{2(R - h_r/2)} \tag{42}$$

$$cos(\theta + \pi/2) = \frac{(c/2)^2 + R^2 - (R + h_r/2)^2}{cR} \tag{43}$$

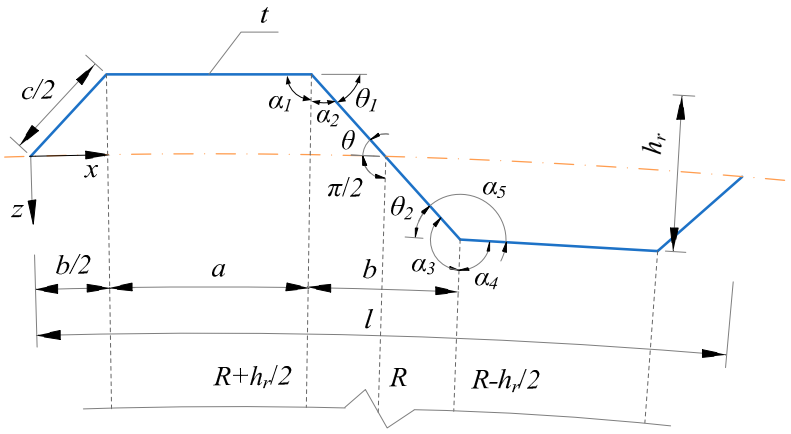

Figure 6. Longitudinal section of a single wavelength PCCSW.

6.5. Angle Relationship of PCCSW

In virtue of the sum of angles being a perigon or straight angle, the equations are as follows:

$$\alpha_5 = 2\pi - \alpha_3 - \alpha_4 \tag{44}$$

$$\theta_2 = \pi - \alpha_5 \tag{45}$$

$$\theta_1 = \pi - \alpha_1 - \alpha_2 \tag{46}$$

In terms of Equations (39), (40) and (46), using inverse operation of the trigonometric function, the expression for the outer folded angle is obtained:

$$\theta_1 = \pi - arccos\frac{a}{2(R + h_r/2)} - arccos\frac{c^2 + 2Rh_r}{2c(R + h_r/2)} \tag{47}$$

In a similar manner, in terms of Equations (41), (42), (44), and (45), the expression for the inner folded angle is obtained:

$$\theta_2 = arccos\frac{c^2 - 2Rh_r}{2c(R - h_r/2)} + arccos\frac{a}{2(R - h_r/2)} - \pi \tag{48}$$

In terms of Equation (43), the expression for the angle of the inclined panel in relation to the tangent line of the longitudinal axis is obtained:

$$\theta = arccos\frac{(c/2)^2 + R^2 - (R + h_r/2)^2}{cR} - \pi/2 \tag{49}$$

6.6. Parametric Analysis and Comparison

To analyze the pure shear global elastic shear buckling behavior of PCCSW, the corrugation dimensions of CSWs for existing bridges [8], given in Table 3, are used. The ratios of parameters for the current analysis of the global shear buckling are:

- Corrugation height-to-thickness ratio: h_r/t = 8–28;
- Web height-to-thickness ratio: H/t = 136–750;
- Ratio of the bending rigidity in the y-direction to that in the x-direction: D_y/D_x = 139–1483;
- Angle of the inclined panel in relation to the tangent line of the longitudinal axis: $\theta = 23.62°$–$39.14°$;
- Outer folded angle: $\theta_1 = 23.83°$–$39.33°$;
- Inner folded angle: $\theta_2 = 23.48°$–$39.02°$;

Table 3. Corrugation dimension of CSWs for existing bridges.

Bridge Name	a (mm)	b (mm)	c (mm)	h_r (mm)
Shinkai	250	200	250	150
Maupre	284	241	284	150
Matsnoki	300	260	300	150
Hondani	330	270	336	200
Iisun	330	330	386	200
Cognac	353	319	353	150
Dole	430	370	430	220

Radius of curvature: R = 30 m–110 m (30 m is the smallest curvature radius of a steel-concrete composite curved bridge [33], which is the most challenging curvature radius for a curved girder bridge with CSWs in the future; 110 m is the minimum curvature radius of the existing curved girder bridge with CSWs, which has already been built in China, namely, Yuwotou Bridge [34] located in Guangzhou, Guangdong).

In the range of the above ratios of parameters, considering the relatively high web height of the bridge, the overall buckling is easy to occur. Additionally, local buckling and interactive buckling are not the main points discussed in this paper, so they are omitted in the data analysis.

It can clearly be observed from Table 4 and Figure 7 that the critical shear stress of the global elastic shear buckling of PCCSW (e.g., for R = 110 m) increases with the increase of panel thickness t and with the reduction of both the height H and the height-to-thickness ratio (H/t). The greater H/t is, the smaller the absolute difference between the theory and finite element values is. Moreover, theoretical values $\tau_{cr,T}$ of the 63 sets of data are in good agreement with the corresponding finite element values $\tau_{cr,F}$ as shown in Table 4 and Figure 8; the mean of the $\tau_{cr,F}/\tau_{cr,T}$ ratios is 1.00, and the covariance is 0.09, and the max and min values are 1.15 and 0.84, respectively. Thus, the accuracy of the theoretical values is verified.

Table 4. Global elastic shear buckling strength of PCCSW with varying height and thickness for R = 110 m. AVE: average value; COV: covariance.

Bridge	H (mm)	t (mm)	H/t	h_r/t	$\tau_{cr,T}$ (MPa)	$\tau_{cr,F}$ (MPa)	$\tau_{cr,F}/\tau_{cr,T}$
Shinkai	2500	10	250	15	1067.81	914.28	0.86
	2500	12	208	13	1171.43	1157.80	0.99
	2500	14	179	11	1267.46	1416.00	1.12
	2700	10	270	15	916.22	887.85	0.97
	2700	12	225	13	1005.13	1126.23	1.12
	3000	8	375	19	664.07	635.54	0.96
	3000	10	300	15	743.34	850.87	1.14
	3500	6	583	25	423.83	410.31	0.97
Maupre	2500	14	179	11	1242.19	1133.89	0.91
	2500	16	156	9	1330.58	1349.98	1.01
	2500	18	139	8	1414.45	1577.02	1.11
	3150	8	394	19	590.98	504.48	0.85
	3150	10	315	15	661.52	674.19	1.02
	3500	8	438	19	480.16	484.50	1.01
	4000	6	667	25	320.08	315.94	0.99

Table 4. *Cont.*

Bridge	H (mm)	t (mm)	H/t	h_r/t	$\tau_{cr,T}$ (MPa)	$\tau_{cr,F}$ (MPa)	$\tau_{cr,F}/\tau_{cr,T}$
Matsnoki	3000	10	300	15	723.65	626.20	0.87
	3000	12	250	13	793.87	793.56	1.00
	3000	14	214	11	858.94	971.79	1.13
	3360	8	420	19	516.81	450.93	0.87
	3360	10	336	15	578.50	600.68	1.04
	3500	8	438	19	476.94	442.29	0.93
	3500	10	350	15	533.86	592.26	1.11
	4000	6	667	25	317.95	288.56	0.91
	4000	8	500	19	367.48	421.28	1.15
Hondani	3000	18	167	11	1535.32	1389.96	0.91
	3000	20	150	10	1620.65	1594.30	0.98
	3000	22	136	9	1702.39	1806.67	1.06
	3600	12	300	17	870.10	769.07	0.88
	3600	14	257	14	940.72	939.17	1.00
	3600	16	225	13	1006.79	1118.26	1.11
	4000	10	400	20	644.70	582.85	0.90
	4000	12	333	17	706.81	739.00	1.05
	4500	8	563	25	457.60	415.81	0.91
	4500	10	450	20	511.95	557.44	1.09
	5000	8	625	25	373.25	399.60	1.07
Iisun	3500	16	219	13	1046.32	940.38	0.90
	3500	18	194	11	1111.19	1099.46	0.99
	3500	20	175	10	1172.94	1266.57	1.08
	3960	12	330	17	708.64	617.80	0.87
	3960	14	283	14	766.16	757.02	0.99
	3960	16	248	13	819.96	904.97	1.10
	4500	10	450	20	503.29	464.78	0.92
	4500	12	375	17	551.78	591.94	1.07
	5000	8	625	25	366.99	333.50	0.91
	5000	10	500	20	410.58	448.70	1.09
	5500	8	688	25	306.21	322.80	1.05
Cognac	3500	10	350	15	525.70	449.89	0.86
	3500	12	292	13	576.71	570.55	0.99
	3500	14	250	11	623.98	699.18	1.12
	4032	8	504	19	356.36	319.54	0.90
	4032	10	403	15	398.89	428.00	1.07
	4500	6	750	25	249.74	210.50	0.84
	4500	8	563	19	288.64	307.08	1.06
Dole	4500	14	321	16	682.03	608.44	0.89
	4500	16	281	14	729.79	723.76	0.99
	4500	18	250	12	774.85	844.56	1.09
	4800	12	400	18	556.39	486.28	0.87
	4800	14	343	16	601.45	594.08	0.99
	4800	16	300	14	643.56	707.62	1.10
	5500	10	550	22	390.71	364.18	0.93
	5500	12	458	18	428.28	462.27	1.08
	6000	8	750	28	296.57	263.02	0.89
	6000	10	600	22	331.75	352.52	1.06
AVE							1.00
COV							0.09
MAX & MIN values							1.15 & 0.84

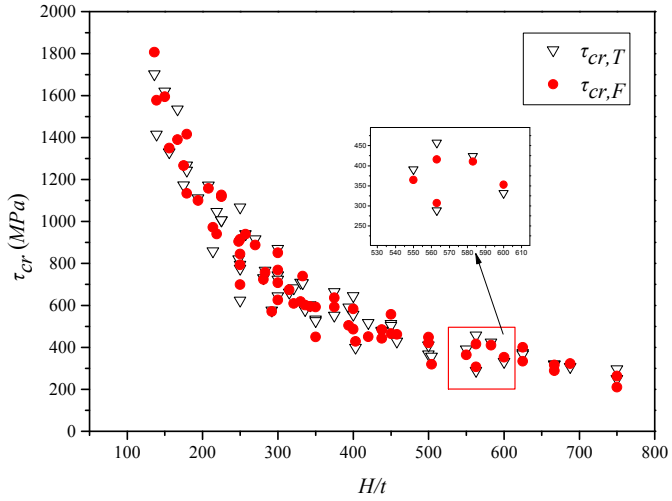

Figure 7. Global elastic shear buckling strength τ_{cr} versus web height-to-thickness ratio H/t (R = 110 m).

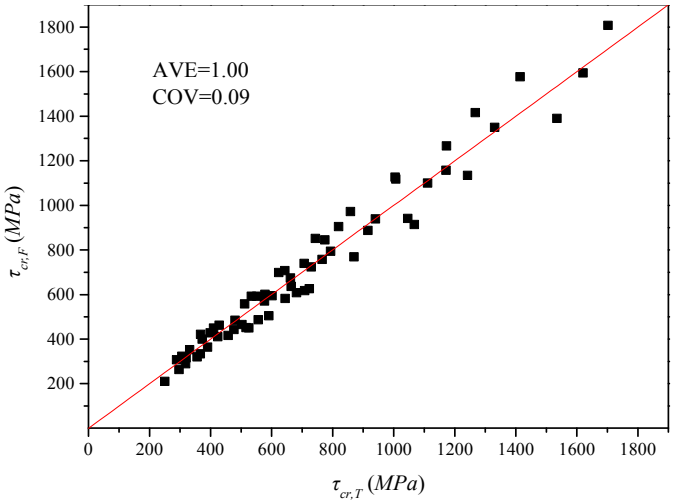

Figure 8. Finite element value $\tau_{cr,F}$ versus theoretical value $\tau_{cr,T}$ of global elastic shear buckling strength. AVE: average value; COV: covariance.

As seen from Figure 9, considering Cognac Bridge as an example, when the radius of curvature and the height of the PCCSW are constant at R = 110 m and H = 4032 mm, the global shear buckling stress of the PCCSW increases with the decrease of aspect ratios a/H and c/H of a single panel (longitudinal panel or inclined panel). It is also clear from the figure that the global shear buckling strength of the PCCSW is more sensitive to c/H than to a/H. This is reasonable as the global buckling involves out of plane deformation for the corrugated web which is resisted by the inclined folds. Hence, changing the width of the inclined folds become greater than that of the longitudinal folds. This result illustrates that for global shear buckling of PCCSW with constant curvature radius and height, the denser the corrugation is, the larger the buckling strength is. It is worth pointing out that these conclusions remain accurate with different corrugation dimensions as the results of the other bridge conditions are qualitatively similar to those of Cognac Bridge.

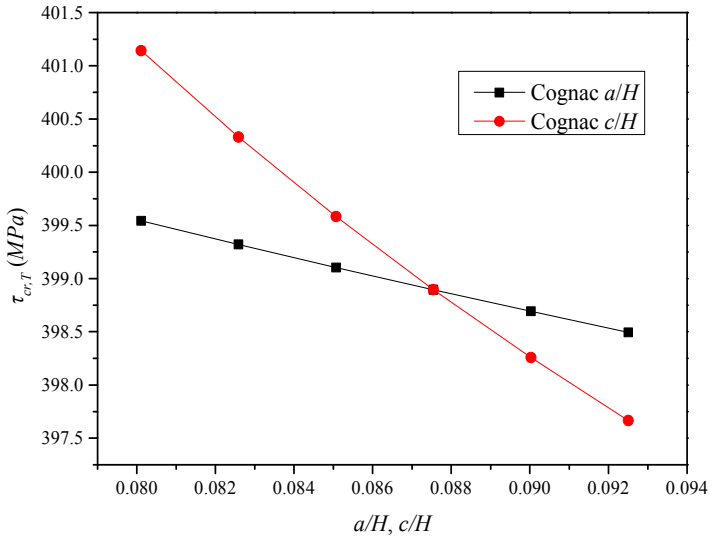

Figure 9. Global elastic shear buckling strength in theory $\tau_{cr,T}$ versus the ratios a/H and c/H (R = 110 m, H = 4032 mm).

As seen from Figures 10–12 and Tables 5 and 6, when the radius of curvature is constant at R = 110 m, it can be concluded that the global shear buckling stress of the PCCSW increases with the increase of the corrugation height h_r. Additionally, the larger the web height-to-thickness ratio H/t is, the slower the growth trend is. Different angles, such as the outer corrugation angle θ_1, the intersection angle θ of the central axis and the inner corrugation angle θ_2 of the PCCSW, also increase with the increase of the corrugation height h_r. Note that the outer corrugation angle θ_1 is greater than the inner corrugation angle θ_2; that is, these angles satisfy the inequality $\theta_1 > \theta > \theta_2$, and the sum of θ_1 and θ_2 is slightly larger than two times θ. It can also be observed that the global shear buckling stress of the PCCSW increases with the increase of the inner and outer corrugation angles and it shows a steady increasing trend. It can also be confirmed that the critical finite element values of the global elastic shear buckling are well matched with the theoretical results, as can be noticed from Table 5.

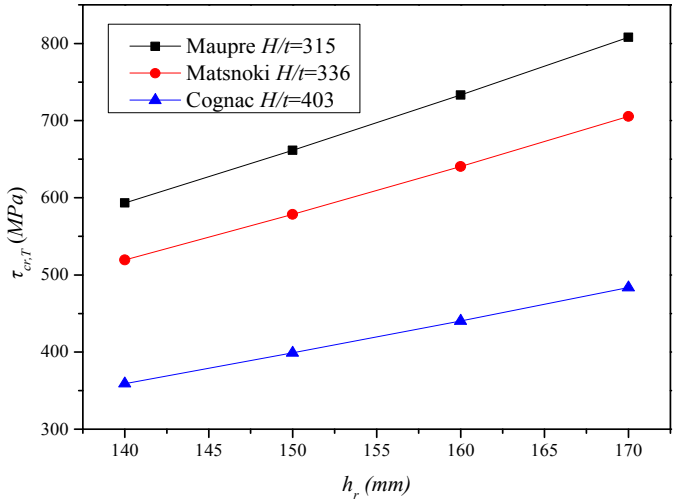

Figure 10. Global elastic shear buckling strength of PCCSW in theory $\tau_{cr,T}$ versus corrugation height h_r (R = 110 m).

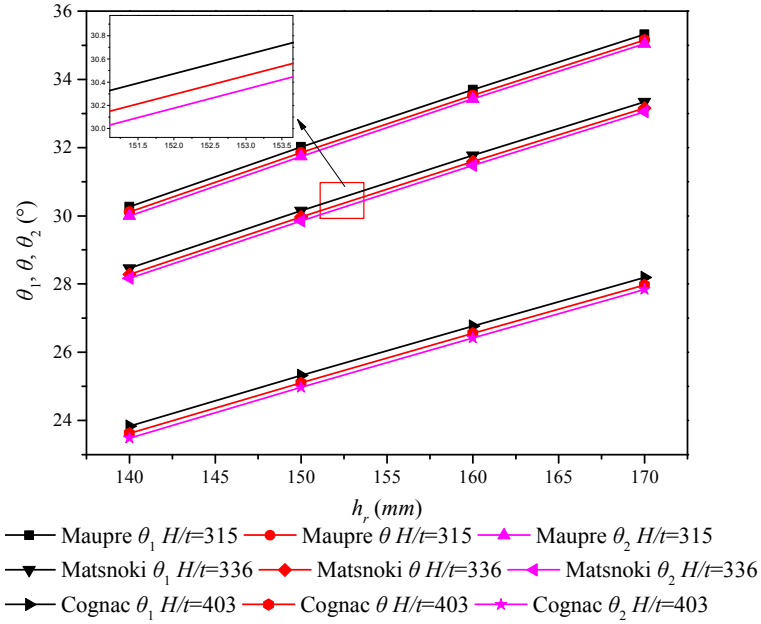

Figure 11. Different angles θ_1, θ and θ_2 versus corrugation height h_r (R = 110 m).

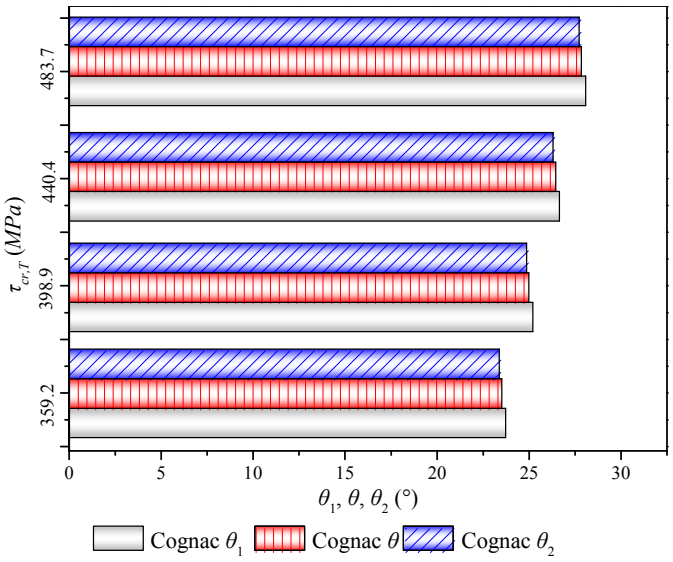

Figure 12. Global elastic shear buckling strength of PCCSW in theory $\tau_{cr,T}$ versus different angles θ_1, θ and θ_2 (R = 110 m).

Table 5. Global elastic shear buckling strength of PCCSW with varying corrugation height for R = 110 m.

Bridge	h_r (mm)	H (mm)	t (mm)	$\tau_{cr,T}$ (MPa)	$\tau_{cr,F}$ (MPa)	$\tau_{cr,F}/\tau_{cr,T}$
Shinkai	130	2700	10	728.09	838.52	1.15
	140	2700	10	819.67	862.85	1.05
	150	2700	10	916.22	887.85	0.97
	160	2700	10	1017.79	902.33	0.89
Maupre	140	3150	10	593.26	654.63	1.10
	150	3150	10	661.52	674.19	1.02
	160	3150	10	733.11	691.87	0.94
	170	3150	10	808.05	707.62	0.88

Table 5. *Cont.*

Bridge	h_r (mm)	H (mm)	t (mm)	$\tau_{cr,T}$ (MPa)	$\tau_{cr,F}$ (MPa)	$\tau_{cr,F}/\tau_{cr,T}$
Matsnoki	140	3360	10	519.32	582.26	1.12
	150	3360	10	578.50	600.68	1.04
	160	3360	10	640.49	617.59	0.96
	170	3360	10	705.32	632.92	0.90
	180	3360	10	772.98	646.58	0.84
Hondani	180	3600	14	794.56	905.24	1.14
	190	3600	14	866.21	923.10	1.07
	200	3600	14	940.72	939.17	1.00
	210	3600	14	1018.13	953.43	0.94
	220	3600	14	1098.44	965.79	0.88
Iisun	180	3960	14	649.19	728.91	1.12
	190	3960	14	706.58	743.58	1.05
	200	3960	14	766.16	757.02	0.99
	210	3960	14	827.93	769.17	0.93
	220	3960	14	891.91	780.10	0.87
Cognac	140	4032	10	359.16	413.22	1.15
	150	4032	10	398.89	428.00	1.07
	160	4032	10	440.41	441.96	1.00
	170	4032	10	483.69	455.03	0.94
	180	4032	10	528.75	467.24	0.88
Dole	200	4800	14	518.84	569.09	1.10
	210	4800	14	559.46	581.95	1.04
	220	4800	14	601.45	594.08	0.99
	230	4800	14	644.81	605.46	0.94
	240	4800	14	689.55	616.09	0.89
AVE						1.00
COV						0.09

Table 6. Global elastic shear buckling strength of PCCSW with different angles and corrugation heights for R = 110 m.

Bridge	θ (°)	θ_1 (°)	θ_2 (°)	H (mm)	t (mm)	hr (mm)	$\tau_{cr,T}$ (MPa)
Shinkai	33.00	33.14	32.91	2700	10	130	728.09
	34.97	35.11	34.87	2700	10	140	819.67
	36.84	36.99	36.75	2700	10	150	916.22
	38.63	38.78	38.54	2700	10	160	1017.79
Maupre	30.11	30.27	30.00	3150	10	140	593.26
	31.85	32.02	31.74	3150	10	150	661.52
	33.53	33.70	33.43	3150	10	160	733.11
	35.15	35.32	35.04	3150	10	170	808.05
Matsnoki	28.28	28.46	28.17	3360	10	140	519.32
	29.97	30.15	29.85	3360	10	150	578.50
	31.59	31.77	31.48	3360	10	160	640.49
	33.16	33.34	33.05	3360	10	170	705.32
	34.68	34.86	34.57	3360	10	180	772.98
Hondani	33.66	33.85	33.53	3600	14	180	794.56
	35.10	35.29	34.98	3600	14	190	866.21
	36.49	36.69	36.37	3600	14	200	940.72
	37.84	38.03	37.72	3600	14	210	1018.13
	39.14	39.33	39.02	3600	14	220	1098.44

Table 6. *Cont.*

Bridge	θ (°)	θ_1 (°)	θ_2 (°)	H (mm)	t (mm)	hr (mm)	$\tau_{cr,T}$ (MPa)
Iisun	28.56	28.77	28.43	3960	14	180	649.19
	29.88	30.09	29.75	3960	14	190	706.58
	31.16	31.38	31.04	3960	14	200	766.16
	32.42	32.63	32.29	3960	14	210	827.93
	33.64	33.85	33.51	3960	14	220	891.91
Cognac	23.62	23.83	23.48	4032	10	140	359.16
	25.10	25.32	24.97	4032	10	150	398.89
	26.56	26.77	26.42	4032	10	160	440.41
	27.97	28.19	27.84	4032	10	170	483.69
	29.35	29.57	29.22	4032	10	180	528.75
Dole	28.38	28.64	28.22	4800	14	200	518.84
	29.57	29.82	29.41	4800	14	210	559.46
	30.72	30.98	30.56	4800	14	220	601.45
	31.86	32.11	31.70	4800	14	230	644.81
	32.96	33.22	32.80	4800	14	240	689.55

As shown in Figure 13, the global elastic shear buckling stress of PCCSW increases with the decrease of the curvature radius R, especially when $R < 60$ m. When the buckling strength is large, the sensitivity of the difference between web height-to-thickness ratios H/t of the two adjacent curves to the absolute difference of the buckling strength becomes great. As noted before, the global elastic shear buckling strength of PCCSW with a small radius of curvature is greater than that of the others. Hence, the absolute shear strength increases obviously, especially for the large CSW with large corrugation dimensions and a small radius of curvature. On the other hand, Figure 14 and Table 7 show that the strength of the CSW used in the curved girder bridge is higher than that of the straight girder bridge. It also illustrates that PCCSW, to some extent, has a stiffening effect on the entire structure under pure shear conditions.

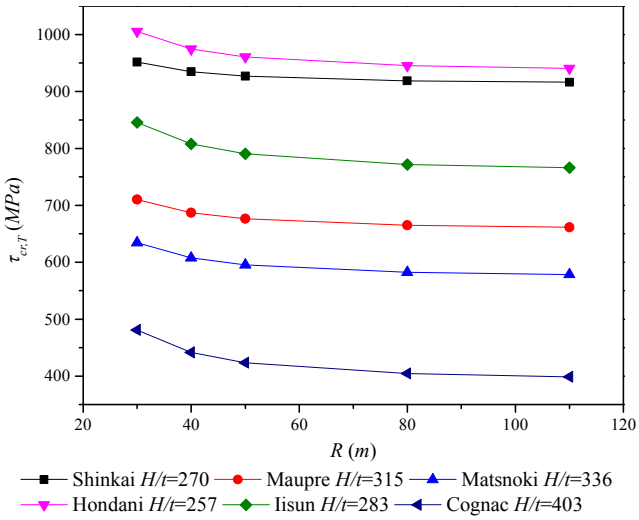

Figure 13. Global elastic shear buckling strength of PCCSW in theory $\tau_{cr,T}$ versus curvature radius R.

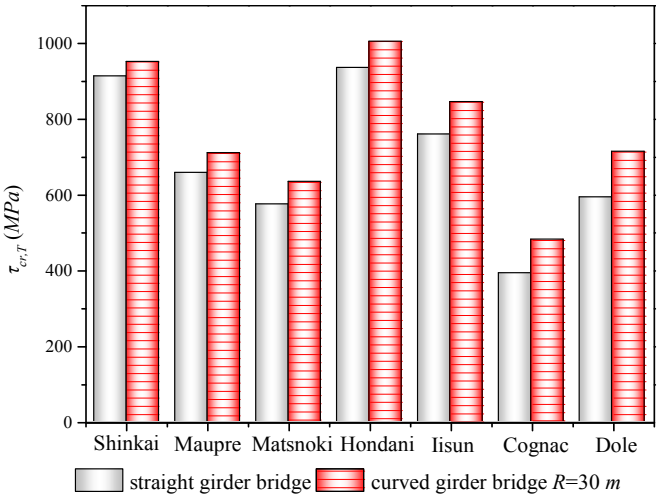

Figure 14. Comparison of global shear buckling strength of a corrugated web used in a straight bridge (R = ∞) and a curved bridge (R = 110 m).

Table 7. Global elastic shear buckling strength of PCCSW with varying curvature radius.

Bridge	R (m)	H (mm)	t (mm)	$\tau_{cr,T}$ (MPa)	$\tau_{cr,F}$ (MPa)	$\tau_{cr,F}/\tau_{cr,T}$
Shinkai	∞	2700	10	913.40	884.19	0.97
	110	2700	10	916.22	887.85	0.97
	80	2700	10	918.74	887.89	0.97
	50	2700	10	927.08	889.85	0.96
	40	2700	10	934.79	892.89	0.96
	30	2700	10	951.53	897.89	0.94
Maupre	∞	3150	10	657.65	673.24	1.02
	110	3150	10	661.52	674.19	1.02
	80	3150	10	664.97	675.21	1.02
	50	3150	10	676.43	677.08	1.00
	40	3150	10	687.06	678.70	0.99
	30	3150	10	710.19	681.11	0.96
Matsnoki	∞	3360	10	574.09	599.82	1.04
	110	3360	10	578.50	600.68	1.04
	80	3360	10	582.43	601.58	1.03
	50	3360	10	595.52	602.26	1.01
	40	3360	10	607.69	603.27	0.99
	30	3360	10	634.22	604.76	0.95
Hondani	∞	3600	14	935.58	937.84	1.00
	110	3600	14	940.72	939.17	1.00
	80	3600	14	945.31	939.76	0.99
	50	3600	14	960.54	940.54	0.98
	40	3600	14	974.66	941.63	0.97
	30	3600	14	1005.39	943.23	0.94
Iisun	∞	3960	14	759.90	755.99	0.99
	110	3960	14	766.16	757.02	0.99
	80	3960	14	771.74	757.43	0.98
	50	3960	14	790.33	757.95	0.96
	40	3960	14	807.60	758.77	0.94
	30	3960	14	845.31	759.94	0.90
Cognac	∞	4032	10	392.50	427.38	1.09
	110	4032	10	398.89	428.00	1.07
	80	4032	10	404.61	428.27	1.06
	50	4032	10	423.72	428.65	1.01
	40	4032	10	441.60	429.14	0.97
	30	4032	10	481.01	429.86	0.89
Dole	∞	4800	14	592.65	593.24	1.00
	110	4800	14	601.45	594.08	0.99
	80	4800	14	609.31	594.46	0.98
	50	4800	14	635.58	594.97	0.94
	40	4800	14	660.12	595.67	0.90
	30	4800	14	714.13	599.96	0.84
AVE						0.98
COV						0.05

As shown in Figures 15 and 16 and Tables 7 and 8, as the radius of curvature R of PCCSW decreases, the outer corrugation angle increases, while the inner corrugation angle decreases. Also, for the same case, the intersection angle of the inclined panel in relation to the tangent line of the longitudinal axis θ decreases slowly, and obviously the outer corrugation angle θ_1 increases faster than that of the inner corrugation angle θ_2. With regard to buckling stress, it can be concluded from Figure 16 that when the radius of curvature R is reduced, the global elastic shear buckling stress of PCCSW increases with the increase of the outer corrugation angle θ_1 and with the reduction of both the intersection angle θ of the central axis and the inner corrugation angle θ_2, and the increasing speed is slower than that of θ_1.

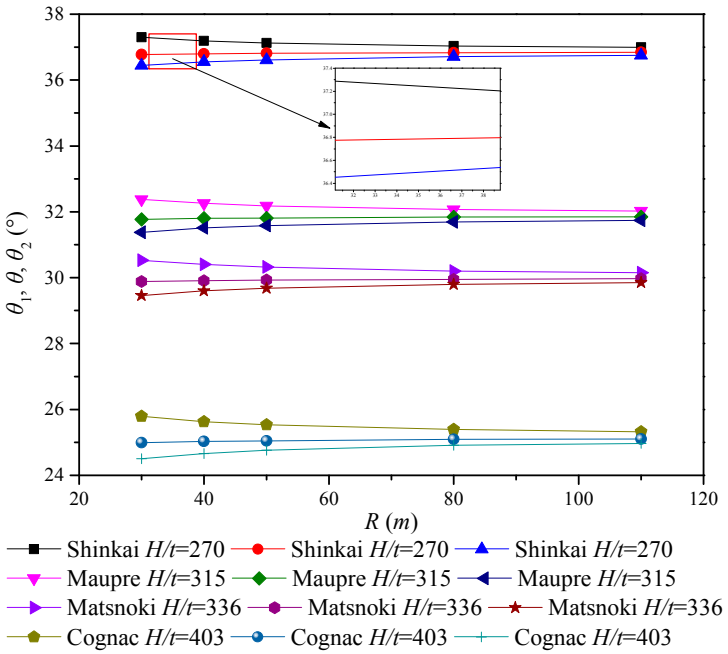

Figure 15. Different angles θ_1, θ and θ_2 versus curvature radius R.

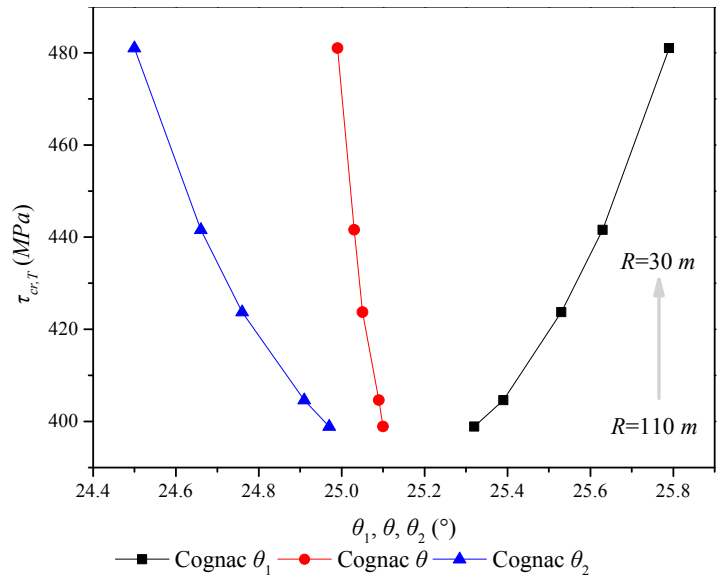

Figure 16. Global shear buckling strength $\tau_{cr,T}$ of PCCSW versus different angles θ_1, θ and θ_2 with varying R.

Table 8. Global elastic shear buckling strength of PCCSW with different angles and curvature radii.

Bridge	θ (°)	θ_1 (°)	θ_2 (°)	H (mm)	t (mm)	R (m)	$\tau_{cr,T}$ (MPa)
Shinkai	36.84	36.99	36.75	2700	10	110	916.22
	36.83	37.03	36.71	2700	10	80	918.74
	36.81	37.13	36.61	2700	10	50	927.08
	36.80	37.19	36.55	2700	10	40	934.79
	36.77	37.30	36.44	2700	10	30	951.53
Maupre	31.85	32.02	31.74	3150	10	110	661.52
	31.84	32.07	31.69	3150	10	80	664.97
	31.81	32.18	31.58	3150	10	50	676.43
	31.80	32.26	31.51	3150	10	40	687.06
	31.77	32.38	31.38	3150	10	30	710.19
Matsnoki	29.97	30.15	29.85	3360	10	110	578.50
	29.95	30.20	29.80	3360	10	80	582.43
	29.93	30.32	29.68	3360	10	50	595.52
	29.91	30.40	29.60	3360	10	40	607.69
	29.88	30.53	29.46	3360	10	30	634.22
Hondani	36.49	36.69	36.37	3600	14	110	940.72
	36.48	36.74	36.31	3600	14	80	945.31
	36.45	36.87	36.19	3600	14	50	960.54
	36.43	36.96	36.10	3600	14	40	974.66
	36.40	37.10	35.96	3600	14	30	1005.39
Iisun	31.16	31.38	31.04	3960	14	110	766.16
	31.15	31.44	30.97	3960	14	80	771.74
	31.11	31.58	30.83	3960	14	50	790.33
	31.09	31.68	30.73	3960	14	40	807.60
	31.05	31.84	30.58	3960	14	30	845.31
Cognac	25.10	25.32	24.97	4032	10	110	398.89
	25.09	25.39	24.91	4032	10	80	404.61
	25.05	25.53	24.76	4032	10	50	423.72
	25.03	25.63	24.66	4032	10	40	441.60
	24.99	25.79	24.50	4032	10	30	481.01
Dole	30.72	30.98	30.56	4800	14	110	601.45
	30.71	31.06	30.49	4800	14	80	609.31
	30.67	31.23	30.31	4800	14	50	635.58
	30.64	31.34	30.20	4800	14	40	660.12
	30.60	31.53	30.01	4800	14	30	714.13

7. Conclusions

In this paper, CSWs in composite curved girders were analyzed by an orthotropic open cylindrical shell modelling. Theoretical derivation of the shear strength and parameter analysis of the global elastic shear buckling behavior of PCCSW was carried out. Based on the detailed study described in this paper, the following conclusions are obtained:

(1) According to the elastic theories of shells and orthotropic materials, the governing differential equations of global elastic shear buckling of PCCSW were given. Through a reasonable dis-placement mode, the critical shear stress of the PCCSW of a composite curved girder was obtained by using the Galerkin method and the variational extremum principle.

(2) The correctness of the proposed theoretical buckling formula was verified by the parametric analysis of a series of finite element models. A comparison of the numerical results of the finite element models with theoretical results showed good agreement. It was found that the denser the corrugation of PCCSW with constant curvature radius and height is, the larger the buckling strength is. Additionally, the global shear buckling strength of PCCSW was found to be more sensitive to the variation of the inclined panel width than to that of the longitudinal panel.

Moreover, the outer folded angle was found to be greater than the inner folded angle, and the sum of the outer and inner folded angles is slightly larger than two times the intersection angle between the inclined panel and the tangent line of the longitudinal axis. Additionally, the results indicated that the global elastic shear buckling stress of PCCSW increases with a decrease in the curvature radius, especially when R < 60 m. Thus, PCCSW has a stiffening effect on the entire structure under the pure shear condition.

(3) Through analysis of the influence of a constant or variable radius of curvature on buckling performance, the following rules were obtained: when the radius of curvature is constant, the smaller the web height and the ratio of web height-to-thickness are or the greater the web thickness and the corrugation height are, the higher the global elastic shear buckling strength of PCCSW is. However, the global shear buckling critical stress of PCCSW increases with a decrease in the radius of curvature of the PCCSW and its inner angle and an increase in the outer folded angle.

(4) By considering the characteristic of PCCSW, namely, there exist a common effect of geometric curvature and orthotropic properties, the effect of these key factors are considered in the calculation of the global elastic shear buckling of CSWs in a composite curved girder for the first time.

Finally, to the authors' opinion, this study can provide a theoretical reference for the design and application of composite curved girders with CSWs, instead of just applying a modification factor for the straight girder's calculations. The applicability of such buckling formula for the use in calculating the ultimate shear strength of curved composite girders is intended in further publication.

Author Contributions: K.W. did the derivation of mechanics modeling, performed the simulations and writing. M.Z., M.F.H. and other authors contributed to the revisions and discussion of the contents.

Funding: This work is financially supported by the National Natural Science Foundation of China (Grants 51378106, 51808559 and 51808323). Their financial support is gratefully acknowledged.

Conflicts of Interest: The authors declare no conflict of interest.

References

1. Jiang, R.J.; Kwong, A.F.T.; Xiao, Y.F. Prestressed concrete girder bridges with corrugated steel webs: Review. *J. Struct. Eng.* **2014**, *142*, 04014108. [CrossRef]
2. Hamilton, R.W. Behavior of Welded Girders with Corrugated Webs. Ph.D. Thesis, Department of Civil Engineering, University of Maine, Orono, Maine, 1993.
3. Sayed-Ahmed, E.Y. Lateral torsion-flexure buckling of corrugated web steel girders. *Proc. Inst. Civ. Eng.-Struct. Build.* **2005**, *158*, 53–69. [CrossRef]
4. Johnson, R.P.; Cafolla, J. Corrugated webs in plate girders for bridges. *Proc. Inst. Civ. Eng.-Struct. Build.* **1997**, *122*, 157–164. [CrossRef]
5. Guo, T.; Sause, R. Analysis of local elastic shear buckling of trapezoidal corrugated steel webs. *J. Constr. Steel Res.* **2014**, *102*, 59–71. [CrossRef]
6. Nguyen, N.D.; Kim, S.N.; Han, S.R. Elastic lateral-torsional buckling strength of I-girder with trapezoidal web corrugations using a new warping constant under uniform moment. *Eng. Struct.* **2010**, *32*, 2157–2165. [CrossRef]
7. Abbas, H.H.; Sause, R.; Driver, R.G. Simplified analysis of flange transverse bending of corrugated web I-girders under in-plane moment and shear. *Eng. Struct.* **2007**, *29*, 2816–2824. [CrossRef]
8. Yi, J.; Gil, H.; Youm, K. Interactive shear buckling behavior of trapezoidally corrugated steel webs. *Eng. Struct.* **2008**, *30*, 1659–1666. [CrossRef]
9. Moon, J.; Yi, J.W.; Choi, B.H. Lateral–torsional buckling of I-girder with corrugated webs under uniform bending. *Thin-Walled Struct.* **2009**, *47*, 21–30. [CrossRef]
10. Kim, K.S.; Lee, D.H. Flexural behavior of prestressed composite beams with corrugated web: Part II. Experiment and verification. *Compos. Part B Eng.* **2011**, *42*, 1617–1629. [CrossRef]

11. Sause, R.; Braxtan, T.N. Shear strength of trapezoidal corrugated steel webs. *J. Constr. Steel Res.* **2011**, *67*, 223–236. [CrossRef]
12. Barakat, S.; Mansouri, A.A.; Altoubat, S. Shear strength of steel beams with trapezoidal corrugated webs using regression analysis. *Steel Compos. Struct.* **2015**, *18*, 757–773. [CrossRef]
13. Easley, J.T. Buckling formulas for corrugated metal shear diaphragms. *J. Struct. Div.* **1975**, *101*, 1403–1417.
14. Galambos, T.V. *Guide to Stability Design Criteria for Metal Structures*; John Wiley & Sons: Hoboken, NJ, USA, 1998.
15. Hassanein, M.F.; Kharoob, O.F. Shear buckling behavior of tapered bridge girders with steel corrugated webs. *Eng. Struct.* **2014**, *74*, 157–169. [CrossRef]
16. Hassanein, M.F.; Kharoob, O.F. Linearly tapered bridge girder panels with steel corrugated webs near intermediate supports of continuous bridges. *Thin-Walled Struct.* **2015**, *88*, 119–128. [CrossRef]
17. Zevallos, E.; Hassanein, M.F.; Real, E.; Mirambell, E. Shear evaluation of tapered bridge girder panels with steel corrugated webs near the supports of continuous bridges. *Eng. Struct.* **2016**, *113*, 149–159. [CrossRef]
18. Hassanein, M.F.; Elkawas, A.A.; El Hadidy, A.M.; Elchalakani, M. Shear analysis and design of high-strength steel corrugated web girders for bridge design. *Eng. Struct.* **2017**, *146*, 18–33. [CrossRef]
19. Leblouba, M.; Barakat, S. Shear buckling and stress distribution in trapezoidal web corrugated steel beams. *Thin-Walled Struct.* **2017**, *113*, 13–26. [CrossRef]
20. Zhou, M.; Zhang, J.; Zhong, J.; Zhao, Y. Shear stress calculation and distribution in variable cross sections of box girders with corrugated steel webs. *J. Struct. Eng.* **2016**, *142*, 04016022. [CrossRef]
21. Zhou, M.; Liu, Z.; Zhang, J.; An, L. Deformation analysis of a non-prismatic beam with corrugated steel webs in the elastic stage. *Thin-Walled Struct.* **2016**, *109*, 260–270. [CrossRef]
22. Zhou, M.; Liu, Z.; Zhang, J.; An, L.; He, Z. Equivalent computational models and deflection calculation methods of box girders with corrugated steel webs. *Eng. Struct.* **2016**, *127*, 615–634. [CrossRef]
23. Basher, M.; Shanmugam, N.E.; Khalim, A.R. Horizontally curved composite plate girders with trapezoidally corrugated webs. *J. Constr. Steel Res.* **2011**, *67*, 947–956. [CrossRef]
24. Bedon, C.; Fragiacomo, M. Numerical and analytical assessment of the buckling behaviour of Blockhaus log-walls under in-plane compression. *Eng. Struct.* **2015**, *82*, 134–150. [CrossRef]
25. Bedon, C.; Amadio, C. Buckling analysis and design proposal for 2-side supported double Insulated Glass Units (IGUs) in compression. *Eng. Struct.* **2018**, *168*, 23–34. [CrossRef]
26. Amani, M.; Edlund, B.L.O.; Alinia, M.M. Buckling and postbuckling behavior of unstiffened slender curved plates under uniform shear. *Thin-Walled Struct.* **2011**, *49*, 1017–1031. [CrossRef]
27. Japan Society of Civil Engineers. *Design Manual for PC Bridges with Corrugated Steel Webs*; Research Committee for Hybrid Structure with Corrugated Steel Webs, Japan Society of Civil Engineers: Tokyo, Japan, 1998. (In Japanese)
28. Monagan, M.B.; Geddes, K.O.; Heal, K.M. *Maple V Programming Guide: For Release 5*; Springer Science & Business Media: Waterloo, ON, Canada, 2012.
29. Timoshenko, S.P.; Gere, J.M. *Theory of Elastic Stability*, 2nd ed.; McGraw-Hill Book Company: New York, NY, USA, 1963.
30. ANSYS. *ANSYS User's Manual Revision 12.1*; ANSYS, Inc.: Canonsburg, PA, USA, 2012.
31. Sayed-Ahmed, E.Y. Composite bridges constructed with corrugated steel web box girders. In Proceedings of the International Symposium-Celebrating Concrete: People and Practice, Dundee, UK, 3–4 September 2003; pp. 43–52.
32. Hassanein, M.F.; Kharoob, O.F. Behavior of Bridge Girders with Corrugated Webs: (I) Real Boundary Conditions at the Juncture of the Web and Flanges. *Eng. Struct.* **2013**, *57*, 554–564. [CrossRef]
33. Lin, W.; Yoda, T. Analysis, design and construction of curved composite girder bridges: State-of-the-art. *Int. J. Steel Struct.* **2010**, *10*, 207–220. [CrossRef]
34. Lei, Z.; Yang, G.; Chen, H. Comparative analysis on main material index of china and international composite girder bridge with corrugated steel web. *World Constr.* **2016**, *5*, 11–19. [CrossRef]